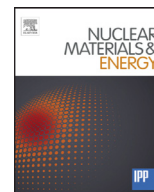




Contents lists available at ScienceDirect

## Nuclear Materials and Energy

journal homepage: [www.elsevier.com/locate/nme](http://www.elsevier.com/locate/nme)

# An inverse method based on finite element model to derive the plastic flow properties from non-standard tensile specimens of Eurofer97 steel

S. Knitel\*, P. Spätig, H.P. Seifert

Laboratory for Nuclear Materials, Nuclear Energy and Safety, Paul Scherrer Institute, 5232 Villigen PSI, Switzerland

## ARTICLE INFO

## Article history:

Received 4 November 2015

Revised 10 June 2016

Accepted 29 June 2016

Available online xxx

## Keywords:

Disk tensile specimens

Inverse method

Finite element simulations

Tempered martensitic steels

Necking behavior

## ABSTRACT

A new inverse method was developed to derive the plastic flow properties of non-standard disk tensile specimens, which were so designed to fit irradiation rods used for spallation irradiations in SINQ (Schweizer Spallations Neutronen Quelle) target at Paul Scherrer Institute. The inverse method, which makes use of MATLAB and the finite element code ABAQUS, is based upon the reconstruction of the load-displacement curve by a succession of connected small linear segments. To do so, the experimental engineering stress/strain curve is divided into an elastic and a plastic section, and the plastic section is further divided into small segments. Each segment is then used to determine an associated pair of true stress/plastic strain values, representing the constitutive behavior. The main advantage of the method is that it does not rely on a hypothetical analytical expression of the constitutive behavior. To account for the stress/strain gradients that develop in the non-standard specimen, the stress and strain were weighted over the volume of the deforming elements. The method was validated with tensile tests carried out at room temperature on non-standard flat disk tensile specimens as well as on standard cylindrical specimens made of the reduced-activation tempered martensitic steel Eurofer97. While both specimen geometries presented a significant difference in terms of deformation localization during necking, the same true stress/strain curve was deduced from the inverse method. The potential and usefulness of the inverse method is outlined for irradiated materials that suffer from a large uniform elongation reduction.

© 2016 The Authors. Published by Elsevier Ltd.

This is an open access article under the CC BY-NC-ND license (<http://creativecommons.org/licenses/by-nc-nd/4.0/>).

## 1. Introduction

The determination of the tensile properties is of primary importance in the assessment of the overall mechanical properties degradation of materials induced by neutron irradiation. The most desirable way to measure those properties is evidently with standard tensile specimens, which guarantee a uniform uniaxial stress and deformation state within the gage section and allow an easy determination of yield stress and post-yield behavior. The standard specimens are usually relatively large and, as such, are not really optimized for irradiations. Over the last decades, there has been a sustained effort to develop small specimen test techniques (SSTT) to measure not only the tensile properties but all the mechanical and physical properties of a broad range of materials under neutron irradiation [1,2]. The main underlying reasons to develop SSTT are the following. First, the volume of most irradiation

facilities is limited. Reducing the size of the specimens is the most straightforward option to increase the number of data that can be obtained in a given irradiation volume. Second, some irradiation facilities, such as the spallation neutron source SINQ [3] at Paul Scherrer Institute or the planned International Fusion Materials Irradiation Facility (IFMIF) [4], are characterized by a strong anisotropic neutron flux. The advantage of using small specimens is to minimize the effects of neutron gradient and associated dose and irradiation temperature gradients through the specimen thickness or length. Third, the handling of big specimens with high residual radioactivity is difficult and cumbersome in hot cells, so that a direct handling of small specimens with low activity is preferable. Furthermore, the minimization of the specimen is often accompanied by the use of exotic specimen geometry as it is the case in this work.

The development of fusion reactor materials requires the qualification of irradiated materials in irradiation environments that are as close as possible to that resulting from deuterium-tritium fusion reactions in terms of neutron and damage spectrum and

\* Corresponding author:

E-mail address: [serafin.knitel@psi.ch](mailto:serafin.knitel@psi.ch) (S. Knitel).<http://dx.doi.org/10.1016/j.nme.2016.06.017>2352-1791/© 2016 The Authors. Published by Elsevier Ltd. This is an open access article under the CC BY-NC-ND license (<http://creativecommons.org/licenses/by-nc-nd/4.0/>).

impurities production. Since there is currently no intense fusion neutron source available, different options have been considered to approach the fusion irradiation conditions [5] and the use of spallation neutron sources is one of them. The irradiation damages produced with spallation facility arise from a mix of neutrons and protons with high energy, which induces a very large transmutation rate. For instance, the helium production per dpa at SINQ spallation facility is about 70 He appm/dpa [6], which is significantly larger than the 10 He appm/dpa expected on the first wall DEMO [5]. While the intrinsic production of impurities is a source of concern, spallation irradiations constitute a great opportunity to investigate the resistance and response of materials to irradiation conditions that are largely unexplored. The design of SINQ target consists of 11 mm diameter stainless tubes and some of them are filled with specimens. The irradiation temperature of the specimens irradiated in SINQ results essentially from the proton beam heating, which unfortunately induces temperature fluctuations on the specimens. To minimize the temperature variations along the centerline of the specimens, their geometry was designed to promote the heat transfer along the radial direction. Thus, the exotic geometry of the so called disk tensile specimens (DTS) used in this work (see below) results from that consideration.

A related difficulty with exotic geometry resides in the fact the constitutive behavior, or equivalently the true stress-strain curve cannot be obtained in a straightforward procedure due to the inhomogeneity of the stresses and strains along the gage length. To extract the constitutive behavior from non-standard specimens, one has to rely on modeling. For instance, an inverse method based on a finite element (FE) model can be used for that purpose. In stress analysis studies, the material elastic and plastic properties are usually known and used as input parameters for FE simulations, along with others boundaries and initial conditions. The output consists of calculated stress and strain fields as well as reaction forces  $F$  and/or displacements  $d$ . An inverse approach uses the opposite direction as this conventional way, i.e., it determines the elastic and plastic properties of the material to use as input for the FE model to reconstruct the measured forces and displacements, e.g. [7]. There are several options to implement an inverse approach. One can adjust the different parameters of a given constitutive equation to fit the measured material behavior or one can reconstruct the constitutive equation in a piece-wise manner by connected small linear segments. Using an analytical expression has the advantage of low computational cost but requires the ability to describe the material by a functional law like Hollomon's or Ludwig's law. An analytical expression for the tempered martensitic was already proposed [8] but such laws are not always well established for technical alloys and are a priori not known for materials after irradiation. Therefore, the advantage of reconstructing the constitutive behavior by segments is that it is applicable to a large class of materials without doing any assumptions on the possible analytical expression of constitutive law.

In this paper an ad-hoc inverse approach to determine the elastic and plastic flow properties of DTS used for irradiation at SINQ is presented.

## 2. Material, experimental procedures and finite element model

The reduced activation tempered martensitic steel Eurofer97 was investigated in this work. This steel is the reference material for the test blanket modules of ITER (International Thermonuclear Experimental Reactor) and contains (wt.%): 9% Cr, 1% W, 0.2% V, 0.14% Ta and 0.12% C. The geometry and size of the used disk tensile specimen is shown in Fig. 1(a)). The nominal gage length  $l_0$  and cross section  $A_0$  of the DTS are respectively 2.06 mm and 1.03 mm<sup>2</sup>. As mentioned above, this circular geometry was so designed to fit the specimen on the radial plane of irradiation tube for SINQ ir-

radiation. All specimens were manufactured by electro-discharge machining. A special gripping system was developed to clamp the specimen and that guaranteed a proper alignment of the DTS. The grips have a 0.3 mm deep recess that enables a pure clamping of the 0.5 mm thick specimen and that at the same time prevents the specimen from slipping. The gripping system and the position of the specimen in the recesses can be seen in Fig. 2. The spacing between the grip brackets is the extended gage length (see Fig. 1(b)) equal to 2.98 mm and matches with the boundary conditions of the FE simulation. The 3D FE model of DTS was built in ABAQUS/CAE 6.14-1 and contains 32,880 linear hexahedral elements of type C3D8R. To catch the strain gradient properly in the shoulder region and during necking, a fine mesh in the extended gage length was used. For the material definition, the Young's modulus  $E$  and the Poisson's ratio  $\nu$  equal to 0.3 are given for the elastic properties and a rate independent isotropic hardening behavior was chosen for the plastic ones. The loading of the specimen is performed in a similar way to the experiment, where one specimen head is clamped and displaced as a whole, while the other head is clamped but remained fixed. A reference point was used to obtain the resulting reaction force in the model.

For comparison, standard round tensile specimens with a 5 mm diameter and a 25 mm gage length were also tested (see Fig. 3). The tensile tests were conducted at room temperature with a Schenck RMC100 machine at constant displacement rates. For the standard specimens, the strain was measured with a clip-on extensometer, while the machine cross-head displacement was used to determine the elongation of the DTS, after correcting for the machine-compliance displacement. In the following, the engineering stress and strain are represented by  $s$  and  $e$ , and the true stress, true strain and plastic true strain by  $\sigma$ ,  $\epsilon$  and  $\epsilon_p$ .

## 3. Inverse finite element procedure

As mentioned above, the aim of the inverse method is to iteratively determine the true stress-strain curve to be used in the FE model to reconstruct the experimental loads and displacements measured on non-standard specimens. In our case, the previous statement means that the calculated and experimental DTS load-displacement curves have to match. If a good agreement is found the material properties are considered determined, but the accuracy depends significantly on the used implementation method. A piece-wise linear reconstruction of the material parameters was chosen.

The inverse piece-wise determination of the true stress-strain curve was performed by considering three different regions of the load-displacement curve of the DTS deformations:

- Region I: Elastic deformation.
- Region II: Plastic deformation up to maximum load and necking onset.
- Region III: Necking to failure.

For ABAQUS FE simulations, the elastic and plastic material properties have to be given as input. In the case of isotropic material like Eurofer97, the elastic properties are fully characterized by two elastic constants. In the region I, the Young's modulus was determined by fitting while the Poisson's ratio was taken as a constant equal. The plastic flow properties were inferred from region II and III, where extensive plasticity occurs. Note that the implementation of isotropic hardening in ABAQUS is simply given by the true flow stress as a function of plastic strain in a tabular form. In other words, the flow properties are represents by means of true stress and plastic strain pairs.

To start the inverse algorithm, the following initial data are required: (i) the experimental engineering stress/strain curve, (ii) an estimate of the Young's modulus  $E$  and proportional limit  $\sigma_0$

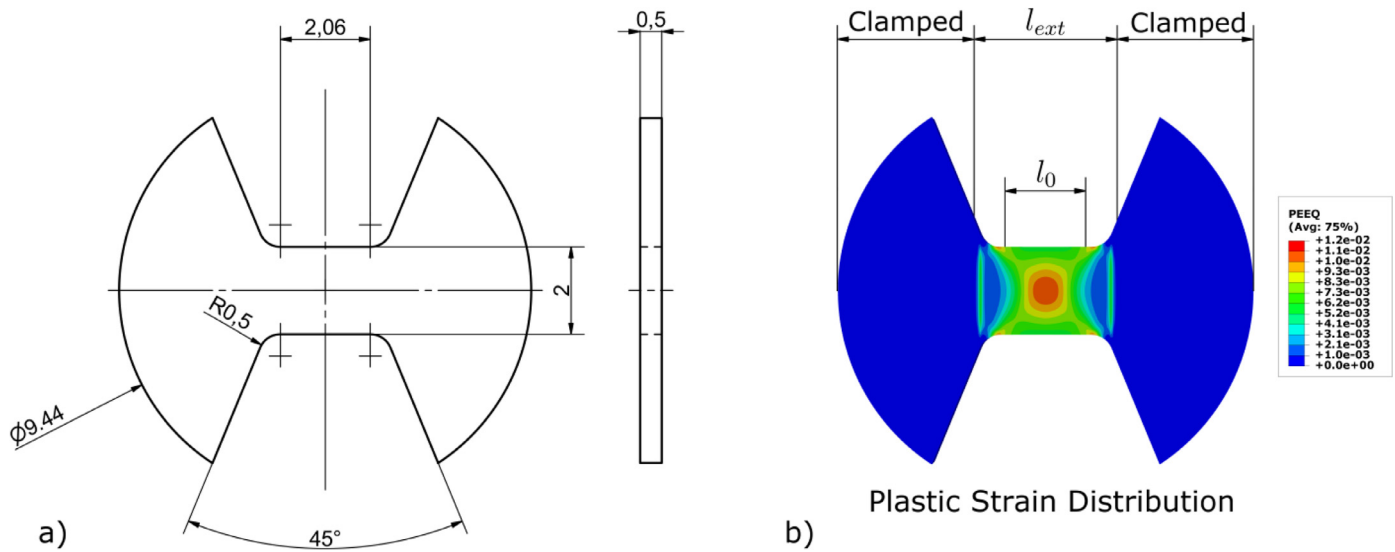


**Fig. 1.** (a) Sketch of the DTS specimen in mm; (b) FE model with the definition of the so-called nominal gage length  $l_0$  and extended gage length  $l_{ext}$ , the clamped areas are also indicated. The equivalent plastic strain (PEEQ) corresponds to a nominal tensile stress of 550 MPa.

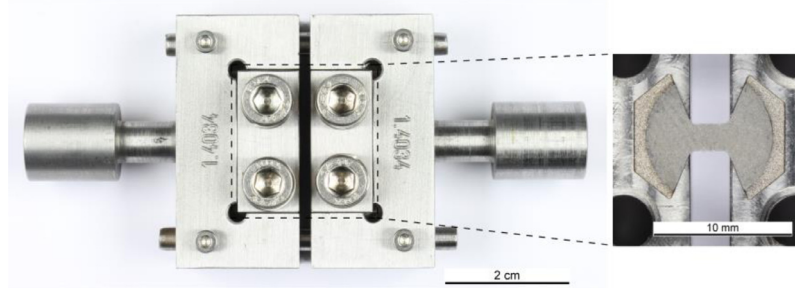


**Fig. 2.** Left: Disk tensile specimen holder; Right: zoom in the clamping areas, showing how the specimen heads lie in the two recesses.

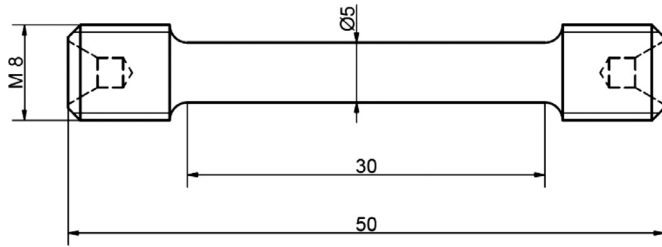


**Fig. 3.** Sketch of the standard round specimen, dimensions in mm.

and (iii) the ABAQUS input file describing the specimen with the boundary and loading conditions. In the following, the piece-wise procedure of the algorithm is described. Even if the goal is to reconstruct the experimental load-displacement ( $P-d$ ) curve of the DTS, for convenience, we have normalized  $P$  and  $d$  by the initial specimen cross-section  $A_0$  and length  $l_0$ . Thus the experimental and simulated data are represented by the engineering stress and engineering strain by Eqs. (1) and (2) respectively:

$$s^{\text{exp}} = P^{\text{exp}}/A_0 \quad e^{\text{exp}} = d^{\text{exp}}/l_0 \quad (1)$$

$$s^{\text{sim}} = P^{\text{sim}}/A_0 \quad e^{\text{sim}} = d^{\text{sim}}/l_0 \quad (2)$$

**Region I:** As mentioned above, for isotropic materials only two elastic constants are necessary to characterize the elastic properties completely. In this work, the Poisson's ratio  $\nu$  was taken equal to 0.3, in agreement with the experimental determination on a

similar tempered martensitic steel [9]. On the contrary the Young's modulus  $E$  was determined with the inverse method. The experimental maximum elastic engineering stress  $e_0^{\text{exp}}$  is naturally defined at the point of the experimental curve where the linearity between  $s^{\text{exp}}$  and  $e^{\text{exp}}$  is lost (see Fig. 4 - left). This point is defined by the pair  $(s_0^{\text{exp}}, e_0^{\text{exp}} = d_{el}/l_0)$ . In an iterative manner, the region I of the  $(s^{\text{sim}} - e^{\text{sim}})$  curve is generated by adjusting the value of the Young's modulus until the following criterion is met:

$$\Delta s = |s_0^{\text{sim}} - s_0^{\text{exp}}| \leq \alpha \quad (3)$$

where  $s_0^{\text{sim}}$  corresponds to the simulated engineering stress at  $d_{el}$  and  $\alpha$  determines the maximum allowable error. So, at the end of the fitting in region I, one has adjusted the Young's modulus to determine  $s_0^{\text{sim}}$ , which is finally converted into  $\sigma_0^{\text{sim}}$ . The algorithm for reconstruction of the true stress-strain curve in the region II can then start. It is important to note here that a direct determination of the Young's modulus from the engineering stress/strain curve of the DTS specimen is not possible, because from the very beginning of the loading the stress state in the specimen is not homogenous and a significant amount of deformation takes place in the specimen shoulders. Hence the slope of linear loading represents only an apparent elastic modulus but not the Young's modulus.

**Region II:** The experimental engineering stress/strain curve is now divided into  $n$  small segments, each of them corresponds to a constant displacement increment  $d_{inc}$  in the load/displacement curve, which of course causes an increment of plastic deformation. For each increment, a corresponding pair of true stress – true plastic strain values can be determined. For the sake of clarity, one provides hereafter the details of the algorithm for the first increment.

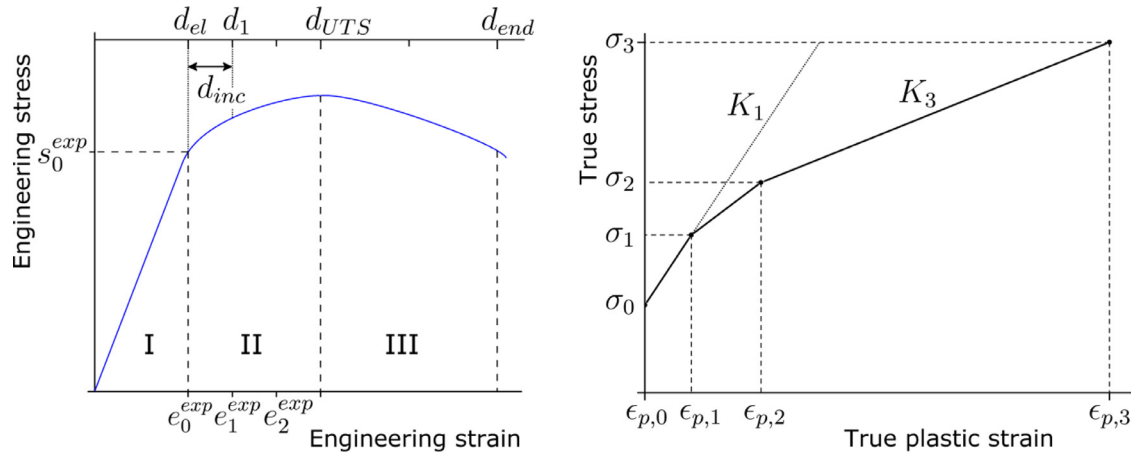


Fig. 4. Left: Engineering stress/strain curve with the three regions. Right: Piece-wise reconstruction of the material properties as (true stress, plastic strain) pairs.

The FE model is updated by imposing a total displacement such as  $d_1 = d_{el} + d_{inc}$ , and by considering a constitutive behavior with a proportional limit equal to  $\sigma_0^{sim}$  (known from the fitting of region 1), followed by plastic behavior characterized by a strain hardening  $K_1$ . The value of this strain-hardening  $K_1$  is obtained when:

$$\Delta s = |s_1^{sim} - s_1^{exp}| \leq \alpha \quad \text{at } d_1 \quad (4)$$

Knowing  $K_1$  is not enough at that point because we are essentially interested in the pair  $(\sigma_1, \epsilon_{p,1})$ .  $\epsilon_{p,1}$  is actually deduced from the FE model by calculating the average true plastic equivalent strain  $\bar{\epsilon}_{p,1}^{sim}$  in the volume of the extended gage length at the simulated displacement  $d_1$  as:

$$\bar{\epsilon}_{p,1}^{sim} = \frac{\sum \epsilon_{p,1}^j V_1^j}{V} = \epsilon_{p,1} \quad (5)$$

where  $\epsilon_{p,1}^j$  is the plastic equivalent strain value in the element  $j$  of volume  $V_1^j$  and  $V$  is the total volume of the extended gage length. The corresponding true stress  $\sigma_1^{sim}$  is simply derived by using the slope  $K_1$  and a linear equation:

$$\bar{\sigma}_1^{sim} = \sigma_0^{sim} + K_1 \bar{\epsilon}_{p,1}^{sim} = \sigma_1 \quad (6)$$

This procedure can be repeated for all subsequent increments  $d_i$  up to the ultimate tensile strength (UTS).

Region III: Beyond UTS, the specimen starts to neck and the deformation becomes localized in a rather small volume. In this region, the procedure to reconstruct the pair of true stress-strain data at the  $i^{th}$  increment is practically the same as in the region II. The slope  $K_i$  is also determined when the criterion  $|s_i^{sim} - s_i^{exp}| \leq \alpha$  is fulfilled for a given  $d_{inc}$ . However, the main difference with respect to region II is that the determination of the average true plastic equivalent strain  $\bar{\epsilon}_{p,i}^{sim}$  at the increment  $i$ , is calculated by considering only the elements whose plastic equivalent strain exceeds that of the previous increment  $i-1$ . In other words, one considers only the region of the specimen that contributes to deformation. Those elements are then used to derive the average plastic equivalent strain  $\bar{\epsilon}_{p,i}^{sim}$  and true stress  $\bar{\sigma}_i^{sim}$  as

$$\bar{\epsilon}_{p,i}^{sim} = \frac{\sum \epsilon_{p,i}^j V_i^j}{\sum V_i^j} = \epsilon_{p,i} \quad (7)$$

$$\bar{\sigma}_i^{sim} = \frac{\sum \sigma_{p,i}^j V_i^j}{\sum V_i^j} = \sigma_{p,i} \quad (8)$$

where  $V_i^j$  is the volume of the element  $j$  which satisfy  $\epsilon_{p,i} > \epsilon_{p,(i-1)}$  and  $\sigma_j$  is the true stress in the element. Due to the fact

that the slope of the flow curve does not change significantly,  $d_{inc}$  can be increased within this region. The procedure is repeated up to failure of the specimen. It is pointed out that the Eqs. (7) and (8) are basically the same as Eqs. (5) and (6). In Eqs. (5) and (6), it is implicitly considered that deformation occurs and increases within all elements of the extended gage, while when necking develops, it is necessary to check which elements undergo deformation.

The implementation of the method consists of the finite element code ABAQUS to calculate the stress/strain and force/displacement fields in the specimen, and of the numerical computing environments MATLAB and Fortran. The MATLAB program is the main controlling program that assures the interface between ABAQUS and Fortran routines, which calculate the average stress and strain within the DTS extended gage length.

The final output of the inverse program yields the proportional limit  $\sigma_0$  and the pairs of true stress/plastic strain in tabular form. We emphasize here that  $\sigma_0$  corresponds to the proportional limit and is not the standard 0.2% offset yield strength. It is well known that the elastic-plastic transition of martensitic steels is very smooth and gradual so that there is a relatively large difference between the proportional limit and yield strength, of the order of 100–150 MPa at room temperature. Therefore, it is important to develop an inverse method that permits to catch the details of the elastic-plastic transition. Indeed, the inverse method will be ultimately applied on irradiated specimens that tend to show a more abrupt transition. A good understanding of the irradiation-induced changes of the plastic behavior and of the onset of the plastic flow demands a careful examination of the elastic-plastic transition, which ultimately plays a role in other mechanical properties. More technically, if the determination of the gradual nature of the transition is overlooked by associating a yield strength value to  $\sigma_0$  then it becomes difficult to properly reconstruct the experimental load-displacement curve. Note that  $d_{inc}$  also affects the quality of flow curve. The larger  $d_{inc}$ , the fewer data points of the flow curve are obtained resulting in a coarse determination of the flow behavior. However, to keep the computational time reasonable while assuring a precise simulation,  $d_{inc}$  was chosen equal to 0.001 mm.

#### 4. Experimental and simulation results

Tests with DTS were performed at room temperature up to failure and the tensile curves in engineering units are presented in Fig. 5 along with the picture of the tested specimens, which all failed in the middle of the gage length. The results show a very good reproducibility, indicating that the developed gripping system was adequate. As expected, the main difference between the



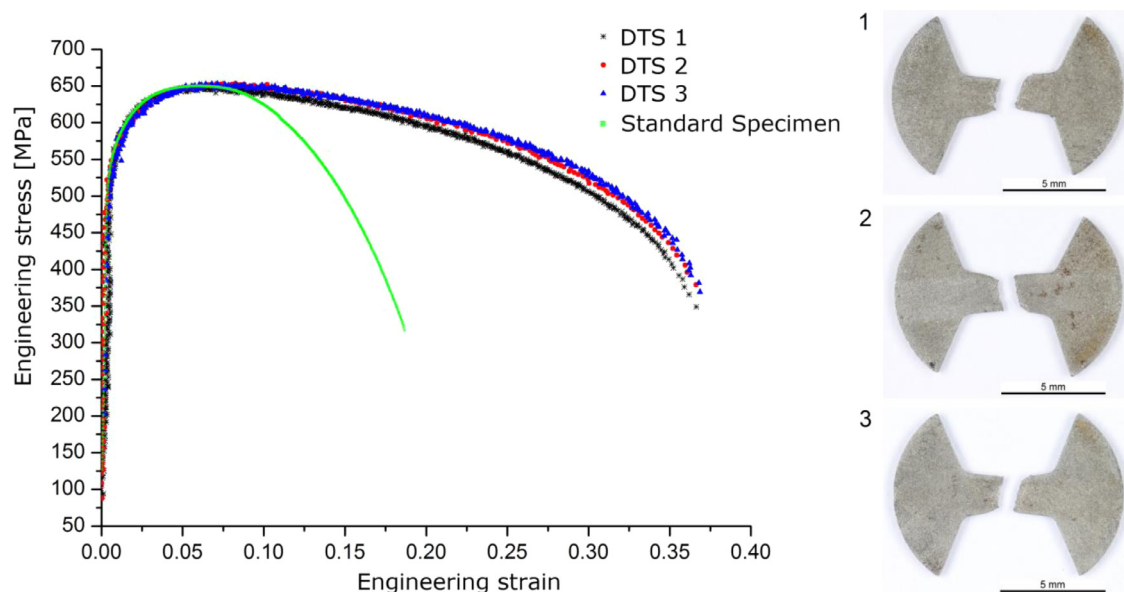


Fig. 5. Standard and DTS curves at room temperature with the corresponding pictures of the tested DTS.

tensile behavior between the DTS and the standard ones resides in the development of the neck. It is however clear that the engineering strain at failure of the standard specimens is much lower than that for the DTS. The engineering strain at failure of the standard specimen is around 20%, in good agreement with published data [10], while it is slightly over 35% for the DTS. This observation is actually expected as it is well known that the total elongation is not a material property but depends on the specimen geometry: the shorter the specimen gage length the larger the relative contribution of the necking region to the total elongation [11].

The curves were further analyzed with the inverse method proposed in this study. Only four initial values have to be given to start the algorithm: the Young's modulus  $E$ , the proportional limit  $\sigma_0$ , the displacement increment  $d_{inc}$  and the maximum allowable error  $\alpha$ . For the initial input values of these parameters the following values were chosen:  $d_{inc} = 0.001$  mm,  $E = 200'000$  MPa,  $\sigma_0 = 380$  MPa and  $\alpha = 1.5$ . With these initial parameters, it takes about 9 hours for the program to reconstruct an entire deformation curve of a tensile test. The fitted value of the Young's modulus was found to be equal 197'187 MPa. This is somewhat lower than the expected value of the Young's modulus value of the 9Cr tempered martensitic steel [9], which lies around 210'000 MPa when measured by ultrasonic wave propagation. The lower Young's modulus determined from the tensile test is likely to arise from an elastic effects and occurrence of micro-plasticity at load below  $\sigma_0$ . One example of DTS engineering stress/strain curve reconstruction is presented in Fig. 6, where in total 44 pairs of  $(\sigma_i, \varepsilon_{p,i})$  were determined. In Fig. 6, one can see that already at low engineering strain level, the deformation in the specimen is quite inhomogeneous.

It can be seen that the discrepancy between the experimental and simulation determined values is very small. Furthermore, one can see in Fig. 6(b)) that the calculated shape of the gage length is in excellent agreement with the experimental at failure. The corresponding true stress-strain data, which again constitute the output of the inverse method, are shown in Fig. 7 as red dots. The largest difference, in the range of 0–5% of plastic strain, is around 0.05% plastic strain and is about 9 MPa, which represents not more than 1.6% of the experimental value. At 5% of plastic strain, UTS is reached and beyond flow properties were obtained by the procedure defined for the region III. In average about 3.1 iteration per pair of  $(\sigma_i, \varepsilon_{p,i})$  were necessary. One emphasizes that with the in-

verse method, the constitute behavior is determined up to large deformation, typical 100% that corresponds to the strain level attained in the neck region. As a matter of fact, the inverse method is also powerful and useful technique to derive the plastic flow at large strain of standard tensile specimens, typically for strains larger than that at necking onset. Furthermore, it is even an avoidable approach to determine the plastic behavior from tensile tests of irradiated tempered martensitic steels. Indeed, the reduction of uniform elongation induced by neutron irradiation is so drastic that the uniform elongation drops down to less than 1%, even for relatively low neutron doses [12]. However, for any stress analysis where plastic deformation occurs, for example in the determination of the near-crack stress field of a component, one has to know the true stress-strain curve over a plastic strain range of 10 to 20%, which corresponds to the plastic strain in the crack tip process zone. In the case of irradiated tempered martensitic steel, this determination can be achieved only by using an indirect method. This approach was already successfully applied by Yamamoto et al. on F82H steel to assess the constraint loss effects in fracture in relation to the strain-hardening capacity of the material [13]. For the sake of comparison, we also plot in Fig. 7 the true stress/strain curve obtained by the inverse method on the standard specimen. The inverse method is clearly consistent, namely yielding the same  $\sigma = \sigma(\varepsilon_p)$  curve for two tensile specimen geometries that exhibit very different necking behavior.

## 5. Conclusions

An inverse approach to determine the flow properties of non-standard disk tensile specimens, used for spallation neutron irradiation at SINQ, was developed. The described approach uses experimental tensile test data, namely the load-displacement curve, and a numerical finite element model to iteratively identify the material constitutive parameters. The Young's modulus, the proportional limit and the strain-hardening are calculated by matching the numerical load-displacement curve to the experimental one. The reconstruction of the load-displacement curve is performed by small linear segments, which avoids making any assumptions on the analytical expression of the strain-hardening of the investigated materials. Hence, the method is quite general. In principle, it can be applied for any isotropic materials with different strain-hardening

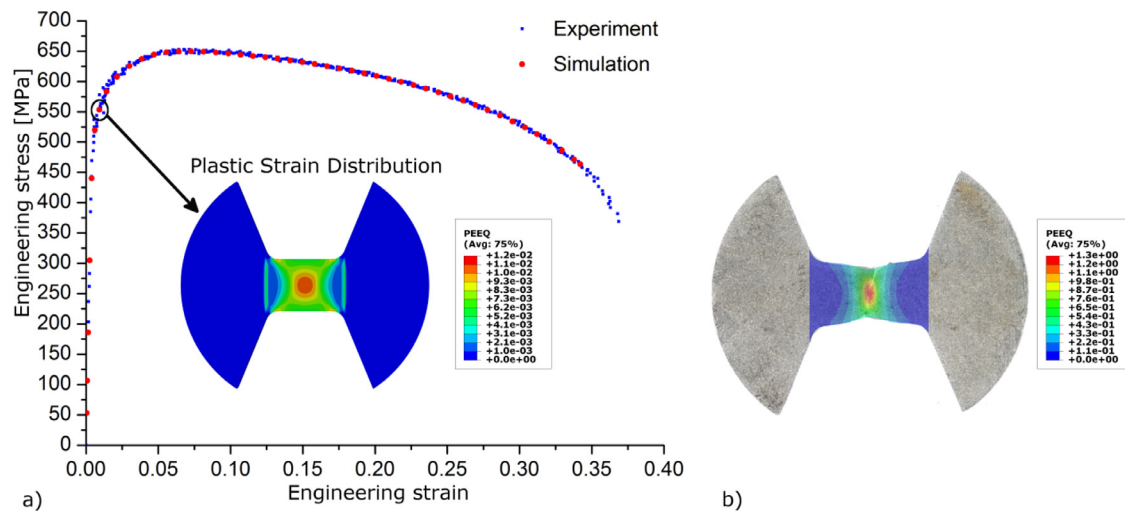


Fig. 6. (a) Experimental and simulated engineering stress/strain curve of DTS, (b) Measured and calculated specimen neck shape at failure displacement.

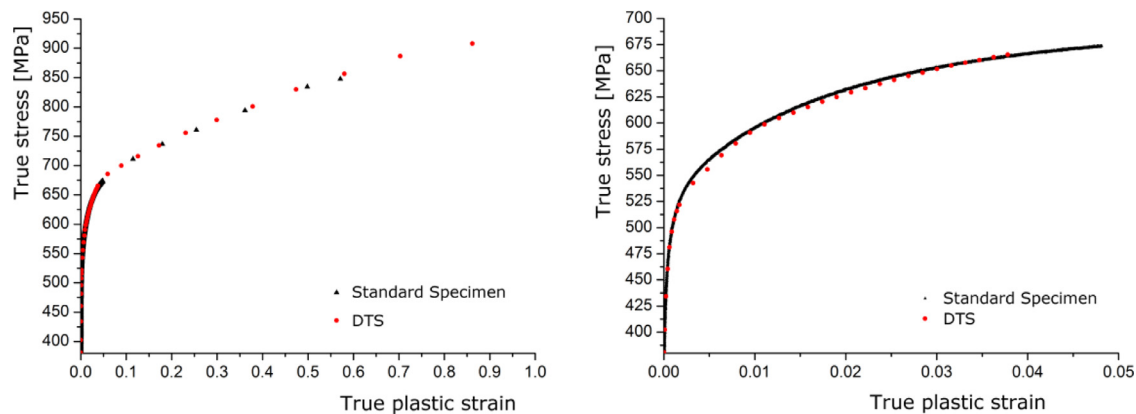


Fig. 7. True stress-strain curve properties by the inverse approach in comparison with experimental data from a standard tensile test.

behaviors. The method was validated by comparing results of the DTS specimens deduced from the inverse technique with tests carried out on standard specimens of Eurofer97 steel. In particular, it was shown that the constitutive behavior can be obtained up to large strain by analyzing the deformation in the neck region. The potential of the inverse method to infer the plastic properties of irradiated tempered martensitic steel with disk tensile specimens that suffer from premature necking was outlined.

## Acknowledgments

The financial support of the [Swiss National Foundation](#) (grant 200020\_159932) is gratefully acknowledged.

## References

- [1] E. Wakai, T. Kikuchi, B. Kim, A. Kimura, S. Nogami, A. Hasegawa, A. Nishimura, M. Soldaini, M. Yamamoto, J. Knaster, *Fusion Eng. Des.* 98–99 (2015) 2089–2093.
- [2] G.E. Lucas, G.R. Odette, H. Matsui, A. Möslang, P. Spätig, J. Rensman, T. Yamamoto, *J. Nucl. Mater.* 367–370 (2007) 1549–1556 Part B.
- [3] W. Wagner, Y. Dai, H. Glasbrenner, H.U. Aebbersold, *J. Nucl. Mater.* 361 (2007) 274–281.
- [4] J. Knaster, S. Chel, U. Fischer, F. Groeschel, R. Heidinger, A. Ibarra, G. Micciche, A. Möslang, M. Sugimoto, E. Wakai, *J. Nucl. Mater.* 453 (2014) 115–119.
- [5] S.J. Zinkle, A. Möslang, *Fusion Eng. Des.* 88 (2013) 472–482.
- [6] Y. Dai, Y. Foucher, M.R. James, B.M. Oliver, *J. Nucl. Mater.* 318 (2003) 167–175.
- [7] G. Sun, F. Xu, G. Li, X. Huang, Q. Li, *Comput. Mater. Sci.* 85 (2014) 347–362.
- [8] P. Spätig, R. Bonadé, G.R. Odette, J.W. Rensman, E.N. Campitelli, P. Mueller, *J. Nucl. Mater.* 367–370 (2007) 527–538 Part A.
- [9] T. Hirose, T. Nozawa, R.E. Stoller, D. Hamaguchi, H. Sakasegawa, H. Tanigawa, H. Tanigawa, M. Enoda, Y. Katoh, L.L. Snead, *Fusion Eng. Des.* 89 (2014) 1595–1599.
- [10] A.A.F. Tavassoli, A. Alamo, L. Bedel, L. Forest, J.M. Gentzmittel, J.W. Rensman, E. Diegele, R. Lindau, M. Schirra, R. Schmitt, H.C. Schneider, C. Petersen, A.M. Lancha, P. Fernandez, G. Filacchioni, M.F. Maday, K. Mergia, N. Boukos, Baluc, P. Spätig, E. Alves, E. Lucon, *J. Nucl. Mater.* 329–333 (2004) 257–262 Part A.
- [11] J.R.D. Associates, in: *Tensile Testing*, 2nd ed., ASTM International, 2004, p. 25.
- [12] N. Ilchuk, P. Spätig, G.R. Odette, *J. Nucl. Mater.* 442 (2013) S58–S61.
- [13] T. Yamamoto, G.R. Odette, M.A. Sokolov, *J. Nucl. Mater.* 417 (2011) 115–119.